Simulating stochastically excited oscillations

The mode lifetime of ξ Hya

Dennis Stello[1,2], Hans Kjeldsen[2,3], Timothy R. Bedding[1], Joris De Ridder[4], Conny Aerts[4], Fabien Carrier[5] and Søren Frandsen[2]
[1] *School of Physics, University of Sydney, NSW 2006, Australia* (stello@physics.usyd.edu.au)
[2] *Department of Physics and Astronomy, University of Aarhus, 8000 Aarhus C, Denmark*
[3] *Teoretisk Astrofysik Center, Danmarks Grundforskningsfond, 8000 Aarhus C, Denmark*
[4] *Instituut voor Sterrenkunde, Katholieke Universiteit Leuven, 3001 Leuven, Belgium*
[5] *Observatoire de Genève, 1290 Sauverny, Switzerland*

Abstract. The discovery of solar-like oscillations in the giant star ξ Hya (G7III) was reported by Frandsen et al. (2002). Their frequency analysis was very limited due to alias problems in the data set (caused by single-site observations). The extent to which the aliasing affected their analysis was unclear due to the unknown damping time of the stellar oscillation modes. In this paper we describe a simulator created to generate time series of stochastically excited oscillations, which takes as input an arbitrary window function and includes both white and non-white noise. We also outline a new method to compare a large number of simulated time series with an observed time series to determine the damping time, amplitude, and limited information on the degree of the stochastically excited modes. For ξ Hya we find the most likely amplitude to be ~ 2 m/s, in good agreement with theory (Houdek and Gough, 2002), and the most likely damping time to be ~ 2 days, which is much shorter than the theoretical value of 15–20 days calculated by Houdek and Gough (2002).

Keywords: asteroseismology, simulation, solar-like oscillations, giant stars, ξ Hya

1. Introduction

The recent detection of solar-like oscillations in the G7 giant star ξ Hya (Stello, 2002; Frandsen et al., 2002) promises new interesting prospects for asteroseismology in this part of the Hertzsprung-Russell diagram. The amplitude spectrum of ξ Hya, based on a one-month time series measured in velocity, showed a clear excess of power within a broad frequency envelope, similar to that seen in the Sun and other solar-type stars (Bedding and Kjeldsen, 2003). The envelope was centered at $\sim 90\,\mu$Hz, as expected from scaling the acoustic cut-off frequency of the Sun (Brown et al., 1991). The highest peak in the amplitude spectrum was ~ 1.9 m/s.

Following these observational results, Houdek and Gough (2002) calculated the theoretical damping rate, η, and amplitude for ξ Hya. The amplitude was ~ 2 m/s and, based on η, we calculated the damping time (or mode lifetime) as $1/(2\pi\eta) \sim 15$–20 days.

The autocorrelation function of the amplitude spectrum of ξ Hya revealed a characteristic frequency separation of $6.8\,\mu$Hz, in good agreement with the expected large frequency separation of the radial modes (i.e. $l = 0$) (Stello, 2002; Frandsen et al., 2002). However, using the frequencies extracted from the observed amplitude spectrum, Stello (2002) showed that a unique solution for the large frequency separation could not be found, due to aliasing. It seemed most likely, however, that the correct value was indeed in the range 6.8–7.0 μHz. The observed frequencies could be explained by purely radial modes, but the presence of non-radial modes could not be excluded, again due to aliasing (Stello, 2002; Frandsen et al., 2002).

Based on a small sample of simulated time series, Stello (2002) showed that the significance of the observed frequencies, due to the effect from aliasing, was strongly dependent on the mode damping time adopted for ξ Hya. Hence, in order to quantify the alias problems, the damping time for ξ Hya has to be known. However, as pointed out by Stello (2002), the damping time of ξ Hya could not be measured directly from the observed amplitude spectrum (by fitting Lorentzian profiles) because the power spectrum was too crowded. Neither was it possible to use the CLEANed spectrum to measure the damping time directly, since the number of frequencies and their position in the spectrum are not known. Therefore, extensive simulations would be needed to estimate the damping time. Furthermore, it should be noted that the preliminary simulations performed by Stello (2002) indicated that the damping time could be significantly shorter than predicted by theory (Houdek and Gough, 2002). It is therefore important to establish a more precise determination of the damping time from the observations than was done by Stello (2002).

In this paper we describe a time-series simulator, outlining the theoretical background and the technique used to simulate stochastically excited oscillations. We use this simulator to determine the damping time of ξ Hya using a new method, which is based on comparing the overall structure of the observed amplitude spectrum with a large sample of simulations. The method also gives the amplitude and some limited information about the mode degree of the oscillations.

The outline of the paper is as follows: Section 2 introduces the fundamental ideas used for simulating the stellar signal from stochastic pulsations, and describes the parameters that the simulator needs as input. Section 3 describes how the simulated time series of ξ Hya were

constructed and outlines how we decided the input parameters. Based on a few results of the simulated data, we introduce in Sect. 4 the method used to determine the damping time of ξ Hya and present an optimum fit to the observations. Finally, we discuss the method and our results in Sect. 5, which also includes the conclusions.

2. Simulator

The simulator described in this paper uses the same fundamental ideas (also described by Chang and Gough (1998)) as the light curve simulator developed for the MONS and Eddington missions (Kjeldsen and Bedding, 1998; De Ridder, 2002; De Ridder et al., 2003).

2.1. Stochastic excitation model

The stellar signal, S, as a function of time, t, is modeled by

$$S(t) = \sum_{\nu=\nu_1}^{\nu_n} s_\nu(t)\,, \tag{1}$$

where each $s_\nu(t)$ is a continuously re-excited damped harmonic oscillator that represents a single oscillation mode.

In general, a damped harmonic oscillator without re-excitation can be expressed as

$$s_\nu(t) = A\sin(2\pi\nu t + \phi)e^{-t/d}\,, \tag{2}$$

where A, ν, ϕ, and d are the amplitude, frequency, phase, and damping time. Rather than assigning a constant amplitude to each oscillator, as in Eq. 2, we instead simulate the re-excitation and damping as a 'kicking' and damping of the amplitude A. The amplitude of each mode is kicked independently at a rate characterized by the small time step, $\Delta t_{\rm kick}$, between each kick. The independence of the re-excitation is established by having different phases, chosen at random, for each mode, so that the time for each kick would not be simultaneous for the different modes. After n kicks the amplitude, A, assigned to a mode is

$$A_n = e^{-\Delta t_{\rm kick}/d}A_{n-1} + \varepsilon_n\,, \tag{3}$$

where $e^{-\Delta t_{\rm kick}/d}$ is the damping factor and ε_n is the nth re-excitation kick, taken at random from a Gaussian distribution with zero mean and standard deviation σ_ε. In order to vary both amplitude and phase in time, we generate the time series as the sum of sine and cosine terms

(using $A\sin(x+\pi/4) = A/\sqrt{2}\,(\sin(x)+\cos(x))$), which are simulated independently. Hence the expression for $s_\nu(t)$ used in this simulator is

$$s_\nu(t) = A_{n,1}\sin(2\pi\nu t + \phi_{\nu,1}) + A_{n,2}\cos(2\pi\nu t + \phi_{\nu,2})\,. \tag{4}$$

The autoregressive process shown in Eq. 3 is asymptotically stable up to second order (i.e. it does not die out or 'explode' as $n \to \infty$), provided $|e^{-\Delta t_{\rm kick}/d}| < 1$, which is always true for physically meaningful values (i.e. $\Delta t_{\rm kick} > 0$ and $d > 0$) (Priestley, 1981). In the asymptotic limit, when the process has relaxed, the mean is $\langle A_n \rangle = 0$, and the variance, $\sigma^2_{A_n}$, can be expressed in terms of σ_ε as

$$\sigma^2_{A_n} \simeq \frac{\sigma^2_\varepsilon}{1 - e^{-2\Delta t_{\rm kick}/d}}\,. \tag{5}$$

Using the amplitude-scaled discrete version of Parseval's theorem (see Kjeldsen and Frandsen, 1992) we have for each term in Eq. 4

$$\begin{aligned} P(\nu) &= 2\frac{1}{N}\sum_{n=1}^{N}|s_\nu(t_n)|^2 \\ &= 2\frac{1}{N}\sum_{n=1}^{N}|A_n|^2|\sin(2\pi\nu t_n + \phi_\nu)|^2 \\ &\simeq \frac{1}{N}\sum_{n=1}^{N}|A_n|^2 \\ &= \sigma^2_{A_n} \end{aligned} \tag{6}$$

for a large number of measurements, N, where $P(\nu)$ is the power at frequency ν in the power spectrum.

Finally, combining Eq. 6 with Eq. 5 gives the value of σ_ε required to simulate a continuously re-excited damped harmonic oscillator, as shown in Eq. 4, that has an average power $P(\nu) = A(\nu)^2$ in the power spectrum. The resulting expression for σ_ε is

$$\sigma_\varepsilon = A\sqrt{\Delta t_{\rm kick}/d}\,, \tag{7}$$

where the first-order approximation of e^x has been used (which assumes $\Delta t_{\rm kick} \ll d$). We obtained Eq. 7 by dividing σ_ε by $\sqrt{2}$ to produce the correct standard deviation of the resulting amplitude for the combined sine and cosine term (cf. Eq. 4).

We repeat the autoregressive process (Eq. 3) for a number of steps that is significantly longer than the characteristic relaxation time, to let it stabilize before the actual simulations of the stellar signal begin. As a rule of thumb, the minimum number of initial steps of the

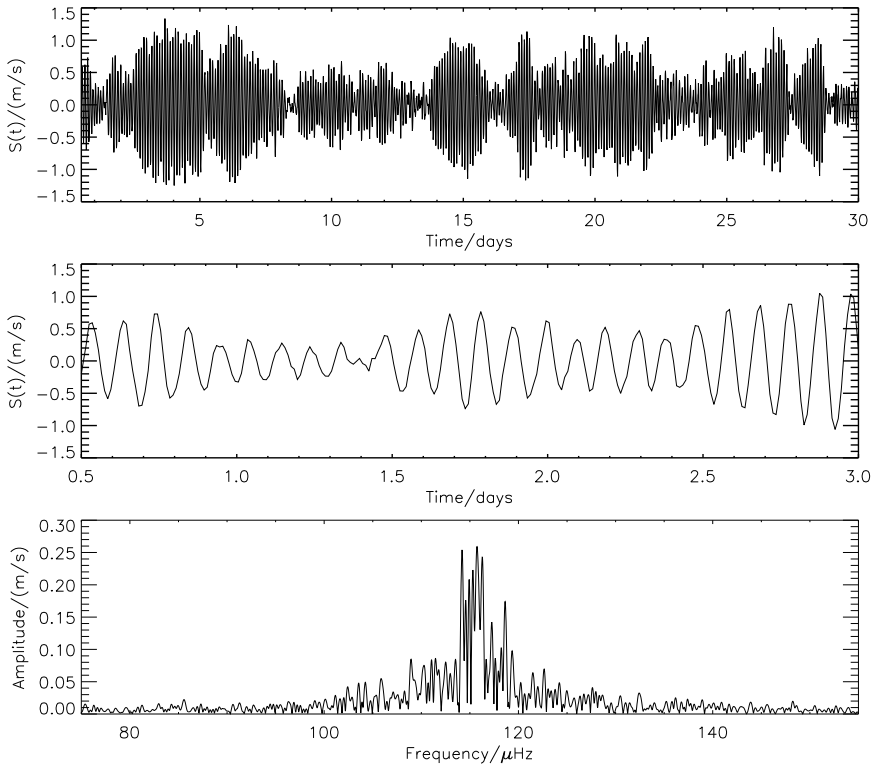

Figure 1. Simulated noise-free time series of a stochastically excited and continuously damped oscillation at a single frequency (Eq. 4). The input parameters are: $d = 1.6$ days, $\nu = 115.7\,\mu$Hz, $A = 0.71$ m/s, and $\Delta t_{\rm kick} = 2$ min. Top panel: Time series of 3000 data points sampled at 14.4 min. Middle panel: Close-up of the upper panel. Bottom panel: Amplitude spectrum of the time series.

autoregressive process (before starting the actual simulations) should correspond to at least twice the damping time.

The simulated signal for each harmonic oscillator described above, $s_\nu(t)$ (Eq. 4), may be viewed as the sum of two vectors in the complex plane. The main vector with length (amplitude) A is anchored at the origin, cycling around it at the frequency of the oscillation. The excitation vector, with variable length, is anchored at the tip of the main vector. Its variable direction relative to the main vector can be separated into the two orthogonal components: phase (orthogonal to the main vector) and amplitude (parallel to the main vector). An example of such a stochastically excited oscillation at a single frequency is shown in Fig. 1. These simulations looks similar to observations of the Sun (Leifsen et al., 2001), which supports the theory of continuous excitation by convective elements (Goldreich and Keeley, 1977; Houdek et al., 1999).

2.2. Amplitude interpolation

The algorithm described in Sect. 2.1 calculates the amplitude (Eq. 3) at regular time steps, but these do not necessarily coincide exactly with the times of the observations. Since the amplitude varies slowly, we simply use the value closest in time to each actual observation. The sinusoidal oscillation itself (Eq. 4), on the other hand, is evaluated at the exact times of the observations. The result is a fast and reliable method for simulating stochastic excited oscillations with an arbitrary observational window function.

2.3. Noise calculation

To make realistic simulations of stochastically excited oscillations, it is very important to be able to include noise (Kjeldsen, 2003). In our simulator both white noise and non-white noise are included.

The white noise is generated by a Gaussian random-number generator. For each data point, the white noise is divided by the weight factor associated with that data point before it is added to the oscillation signal.

The non-white noise is created by first calculating the Fourier spectrum of a white noise source generated by a random generator. Then we multiply it by a function that describes the desired profile of the non-white noise. The result is then converted back to the time domain, producing the time series of the non-white noise source, which finally is added to the oscillation signal.

2.4. Input parameters

To summarize, the following input parameters have to be supplied to the simulator:

1. A set of frequencies.
2. The amplitude corresponding to each frequency.
3. The damping time corresponding to each frequency.
4. The time of each observation (the observational window).
5. The weight of each observation.
6. A set of parameters defining the noise levels according to the chosen noise function.
7. The time step between each re-excitation kick $\Delta t_{\rm kick}$.

3. Simulating time series of ξ Hya

We used the simulator described in Sect. 2 to generate a large number of time series similar to that obtained for ξ Hya by Frandsen et al. (2002). The input parameters for the simulator were as follows:

1. Since the observations can be explained as purely radial modes (Stello, 2002; Frandsen et al., 2002), this simple case has been chosen for the main part of the current investigation. The input frequencies, $\nu_1, \ldots, \nu_n$, were the radial modes from a pulsation model (Stello, 2002), rescaled so that the mean frequency separation was $6.8\,\mu$Hz, in agreement with the observations (Stello, 2002; Frandsen et al., 2002).

2. The relative amplitude of each mode was defined according to an envelope (see Fig. 2, solid vertical lines). The envelope was obtained by smoothing the observed amplitude spectrum, subtracting the noise background and normalizing the peak to unity. In order to match simulations with observations the width of the envelope was made adjustable. We chose to do this by raising the curve to the xth power, where x was a free parameter, which was a convenient way of changing the width of the envelope without changing the height. The envelope was then scaled vertically by a factor $\mathrm{Amp}_{\mathrm{scale}}$, which was a free parameter that represents the oscillation amplitude of ξ Hya. Figure. 2 (dashed curve) shows the normalized envelope for $x = 2$ and $\mathrm{Amp}_{\mathrm{scale}} = 1\,\mathrm{m/s}$.

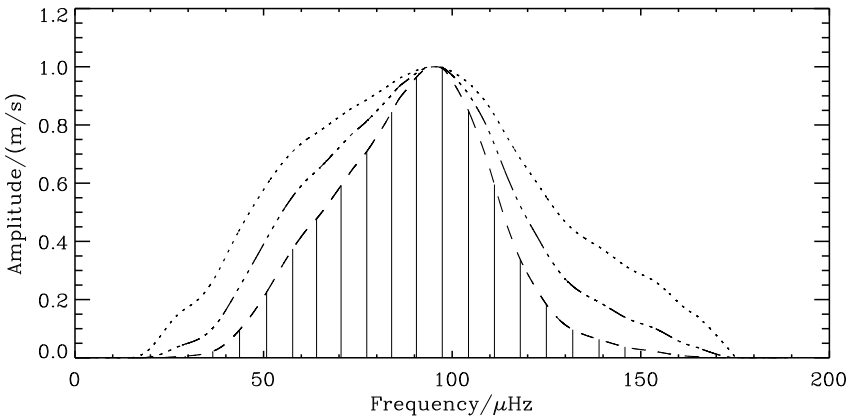

Figure 2. Three amplitude envelopes: dashed curve: $x = 2$ ($\mathrm{FWHM_{in}} = 48.0\,\mu$Hz); dashed-dot-dot-dot curve: $x = 1.2$ ($\mathrm{FWHM_{in}} = 64.0\,\mu$Hz); dotted curve: $x = 0.7$ ($\mathrm{FWHM_{in}} = 81.6\,\mu$Hz). The vertical solid lines indicate the mode frequencies.

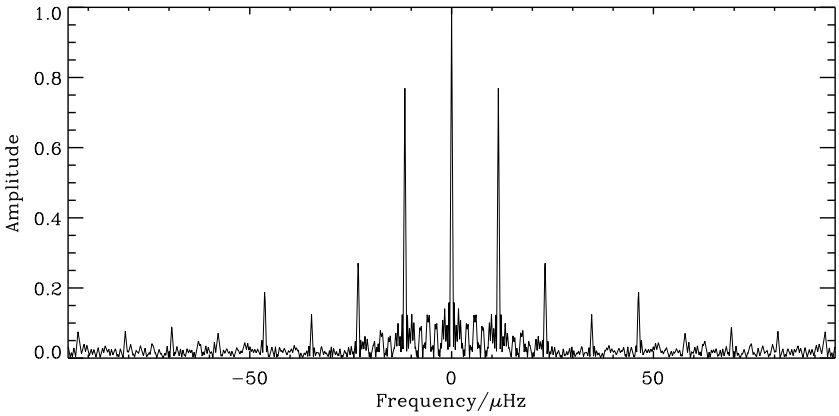

Figure 3. Spectral window of the ξ Hya time series.

3. The damping time, d, was a free parameter and was the same for all modes. This is probably a reasonable approximation, since the theoretical damping rate shows a flat plateau covering a fairly broad range of frequencies ($\sim$ 70–130 μHz) (Houdek and Gough, 2002).

4. The observational window function was exactly the same as for the actual observations (Stello, 2002; Frandsen et al., 2002). The amplitude spectrum of the observational window (the spectral window) is shown in Fig. 3.

5. The weight of each observation was $1/\sigma_i^2$, where σ_i was the noise associated with each observed data point.

6. The noise was the sum of a white and a non-white noise component, where the latter was described by a linear model. The noise was therefore specified by three parameters: the white noise level ($\mathrm{Noise_{white}}$), the slope of the non-white noise ($\mathrm{Noise_{slope}}$), and a scaling of the non-white noise ($\mathrm{Noise_{scale}}$).

7. The time step Δt_{kick} was set to 2 min to meet the requirement that $\Delta t_{\mathrm{kick}} \ll d$ for all damping times tested in this investigation.

Before starting the actual simulations, we repeated the autoregressive process (Eq. 3) for 120000 steps, corresponding to 167 days, which is significantly longer than the characteristic relaxation time for all the damping times tested in this investigation, to ensure it had stabilized.

4. Method and results

Examples of simulated amplitude spectra with different damping times are shown in Fig. 4. It is clear that amplitude spectra based on a short damping time have much more densely packed peaks (top panel) than do those with long damping times (bottom panel). This arises

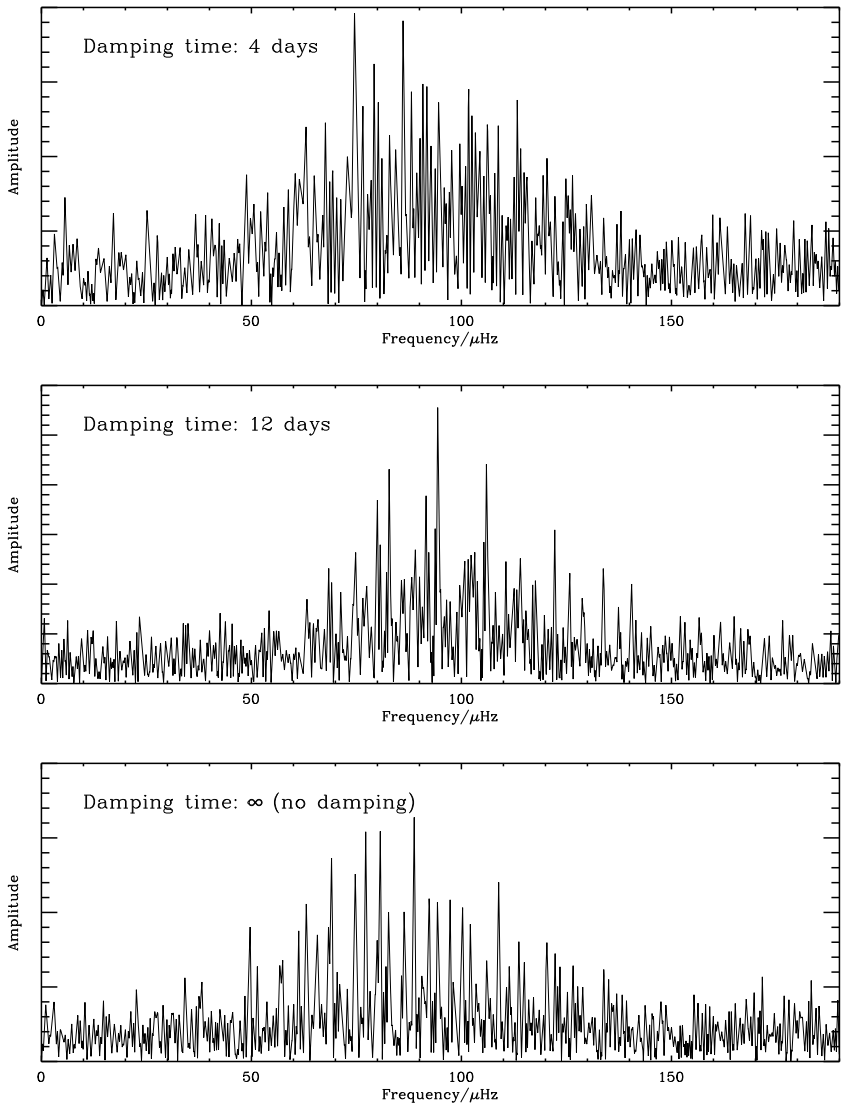

Figure 4. Amplitude spectra based on simulated time series. The input damping times for the time series are shown in each panel. For infinite damping time (bottom panel) the input amplitudes were randomized.

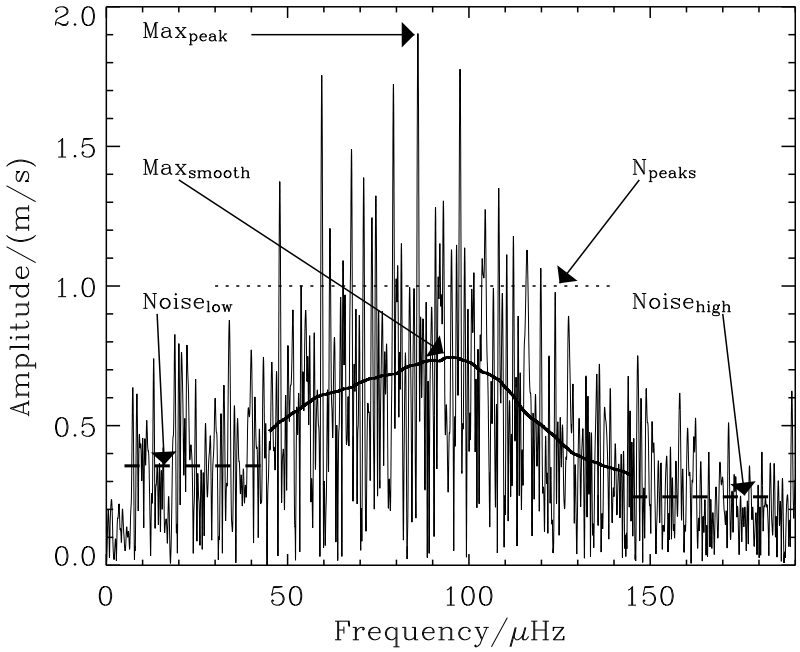

Figure 5. Amplitude spectrum (observed) of ξ Hya. Different parameters characterizing the spectrum are indicated (see text page 10).

because the continuous re-excitation of modes introduces slight shifts in the phase as a function of time, which shows up in the amplitude spectrum as extra peaks slightly offset in frequency. The fact that amplitude spectra based on different damping times display such different characteristics, as seen in Fig. 4, suggests the possibility of measuring the mode damping time from the overall structure of the amplitude spectrum.

We determined how well the simulated time series reproduced the observations by using eight measurable parameters that characterized different features of the amplitude spectra. In Fig. 5 we show the observed amplitude spectrum of ξ Hya, together with the measurable parameters that specify different characteristics of the amplitude spectrum.

The highest peak ($\mathrm{Max_{peak}}$) is the highest amplitude found in the spectrum, while $\mathrm{Max_{smooth}}$ is the height of the smoothed amplitude spectrum, where smoothing was done twice with a boxcar filter. The widths of the boxcars were $20\,\mu$Hz followed by $5\,\mu$Hz. The two noise levels, $\mathrm{Noise_{low}}$ and $\mathrm{Noise_{high}}$ are measured as the mean amplitude

in the frequency ranges 5–45 μHz and 145–185 μHz, respectively. The number of detected peaks with amplitudes above a threshold of 1.0 m/s (S/N$\geq$ 3.5), denoted N_{peaks}, is found by CLEANing the amplitude spectrum until the amplitude threshold has been reached. Our CLEAN process subtracts one frequency at a time (the one with the highest amplitude), but recalculates the amplitude, phase and frequencies of the previously subtracted peaks while fixing the frequency of the latest extracted peak. In this way, the fit of sinusoids to the time series is done simultaneously for all peaks. The mean amplitude is measured both over the entire frequency range 0–190 μHz (Amp_{tot}) and in the central part that is dominated by the stellar excess of power, 40–140 μHz (Amp_{cen}). Finally, the width of the excess power (W_{env}) is measured as the FWHM of the smoothed spectrum after the noise has been subtracted. Due to the window function, stellar excess power 'leaks' into the frequency regions where we measure the noise. The subtraction of noise in the determination of the envelope width therefore includes some stellar power, making W_{env} smaller than the input widths (Fig. 2), which therefore should not be compared.

We now describe how the eight parameters measured from the simulated amplitude spectra (Max_{peak}, Max_{smooth}, $Noise_{low}$, $Noise_{high}$, N_{peaks}, Amp_{cen}, Amp_{tot}, W_{env}) are affected by changes in the input parameters, namely damping time (d), noise ($Noise_{white}$, $Noise_{slope}$, $Noise_{scale}$), amplitude (Amp_{scale}), envelope width (determined by the exponent x), and input frequencies ($\nu_1, \ldots, \nu_n$).

4.1. Damping time

Figure 6 shows the dependence of each of the eight measured parameters on the damping time. Values adopted for the other input parameters are given in the figure caption. Each plotted point is the mean of 100 simulations with the same input parameters but different random number seeds, and the vertical bars show the rms scatter over these 100 simulations. This rms is the intrinsic scatter due to the stochastic nature of the oscillations, and is therefore the quantity we should use to decide whether the simulations match the observations. The parameters measured from the observed amplitude spectrum are indicated by horizontal dashed lines.

All the parameters increase as the damping time gets shorter except for Max_{peak}, which falls off. The fall in Max_{peak} is simply because the re-excitation spreads the power over more peaks, giving less power in each. The relative change in most of the parameters over the range of damping times plotted in Fig. 6 is fairly small ($\lesssim 10\%$) and is generally less than the rms scatter. These parameters are therefore not very sen-

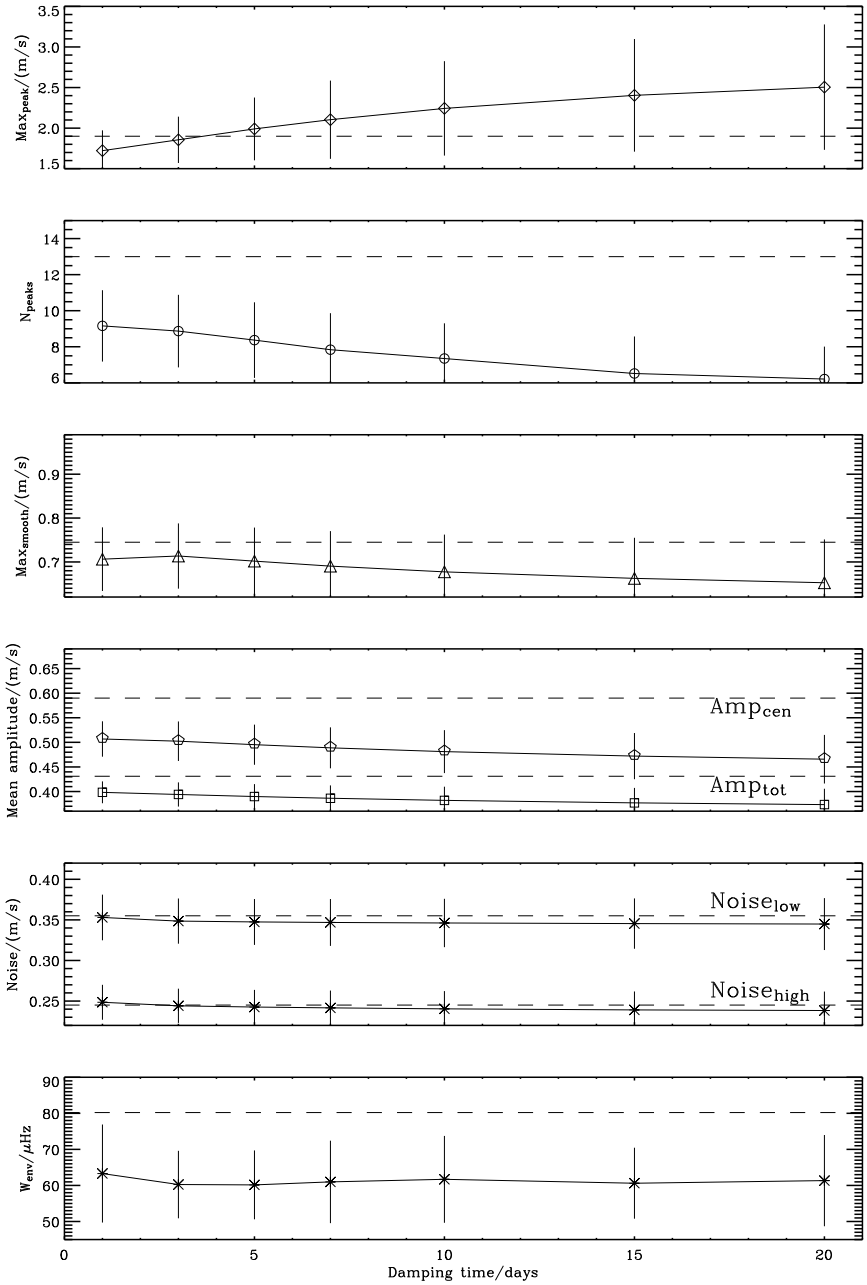

Figure 6. The eight measured parameters as a function of the damping time. The data points are based on 7 distinct sets of simulated spectra only differing in their damping time. Each set comprised 100 independent simulated time series. Each plotted point is the mean of the values found from the 100 simulations within each set, and the vertical bars indicate the rms scatter that results from the stochastic nature of the simulation. The points are connected by solid lines to guide the eye. The *dashed lines* denote the values measured from the observations. The common input parameters for the 7 sets are: $\mathrm{Amp_{scale}} = 2.1\,\mathrm{m/s}$, $x = 2.0$ ($\mathrm{FWHM_{in}} = 48.0\,\mu\mathrm{Hz}$), $\mathrm{Noise_{white}} = 0.20\,\mathrm{m/s}$, $\mathrm{Noise_{slope}} = 1.5$, $\mathrm{Noise_{scale}} = 3.0$, and 18 input frequencies with a mean frequency separation of $6.8\,\mu\mathrm{Hz}$.

sitive measures of the damping time but should still be matched with the observed values to constrain the other input parameters. However, $\mathrm{Max_{peak}}$ and $\mathrm{N_{peaks}}$ change by roughly 50% in the same range and in opposite directions, making them the obvious parameters of choice for constraining the mode damping time. The correlation coefficient between $\mathrm{Max_{peak}}$ and $\mathrm{N_{peaks}}$ is only $\rho \sim 0.10$–0.15, based on a few sets of 100 simulated amplitude spectra, where each set had different input parameters. These two parameters can therefore be regarded as uncorrelated.

The 2nd, 3rd, and 4th panels in Fig. 6 all indicate that, for all damping times, the amount of power in these simulations is too low. The bottom panel shows that this is partly because the width is too narrow. The input power can be adjusted by changing the input noise, amplitude, envelope width, and the number of frequencies (their mean separation). We address each of these possibilities in turn in the next sections.

4.2. Noise

We investigated how the measured parameters changed as a function of input noise. We only show the results of changes in $\mathrm{Noise_{white}}$ because this parameter gave us all the control we needed to adjust the simulations to match the noise level in the observations. The two other noise parameters were fixed at the values used for Fig. 6.

Figure 7 shows that the parameters most sensitive to changes in the input noise are $\mathrm{Noise_{low}}$ and $\mathrm{Noise_{high}}$, while the other parameters show much smaller changes. The input noise can therefore be regarded as the final fine tuning parameter, and has less importance for constraining the other input parameters. The panel showing the measured noise will therefore be omitted in the following plots.

4.3. Amplitude

In Fig. 8 we show the dependence of the measured parameters on the input amplitude. It can be seen that all parameters show an increase with input amplitudes, which is expected due to the increase in power, although the change is very small for $\mathrm{W_{env}}$.

It is clear from Fig. 8 that the input amplitude is constrained by $\mathrm{Max_{peak}}$, which should not be too high, and by $\mathrm{N_{peaks}}$, which should not be too low. The difficulty in satisfying both constraints simultaneously becomes greater for larger values of the damping time.

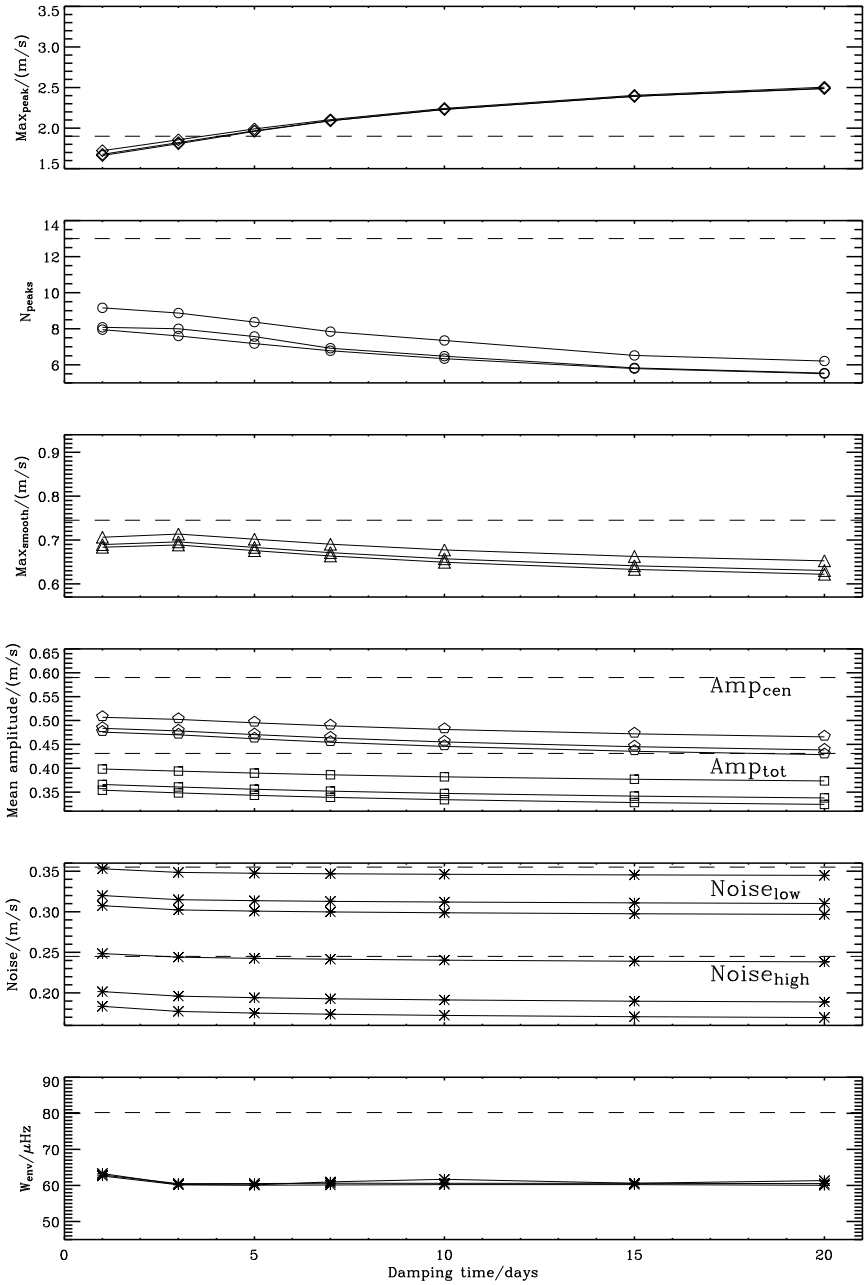

Figure 7. The effect of changing the white noise. These panels are similar to those plotted in Fig. 6, but for three different values of the white noise. Each measured parameter is therefore shown as three points for every damping time. The values for input noise (from top to bottom in each panel) are: $\mathrm{Noise_{white}} = 0.2\,\mathrm{m/s}$ (as in Fig. 6), $\mathrm{Noise_{white}} = 0.1\,\mathrm{m/s}$, and $\mathrm{Noise_{white}} = 0.0\,\mathrm{m/s}$. All parameters show an decrease as $\mathrm{Noise_{white}}$ decreases. Note that the y-axis has been shifted, but not scaled, relative to Fig. 6. For clarity, the vertical bars indicating rms scatter have been omitted.

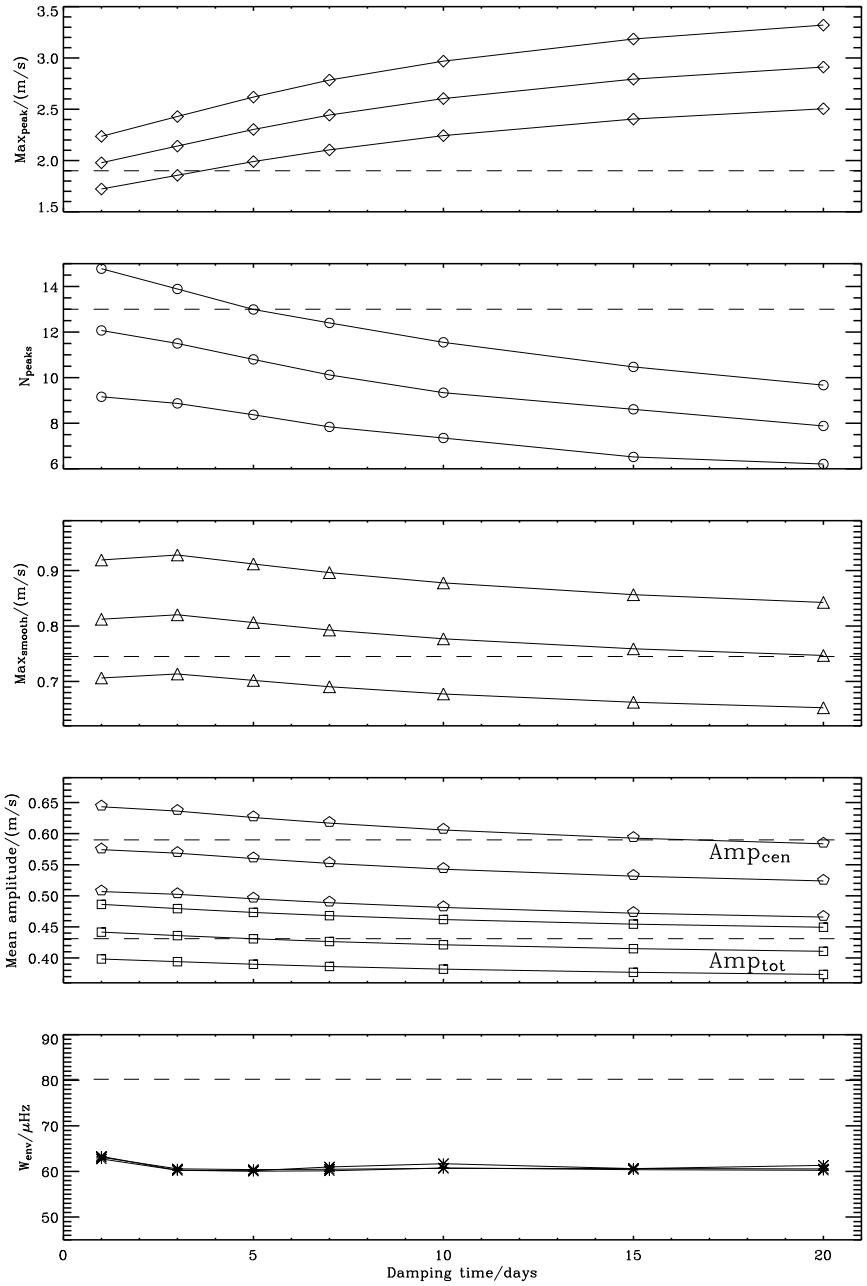

Figure 8. The effect of changing the input amplitude. These panels are similar to those plotted in Fig. 6, but for three different values of input amplitude. Each measured parameter is therefore shown as three points for every damping time. The input amplitudes (from bottom to top in each panel) are: $\mathrm{Amp_{scale}} = 2.1\,\mathrm{m/s}$ (as in Fig. 6), $\mathrm{Amp_{scale}} = 2.5\,\mathrm{m/s}$, and $\mathrm{Amp_{scale}} = 2.8\,\mathrm{m/s}$. All parameters show an increase as $\mathrm{Amp_{scale}}$ increases.

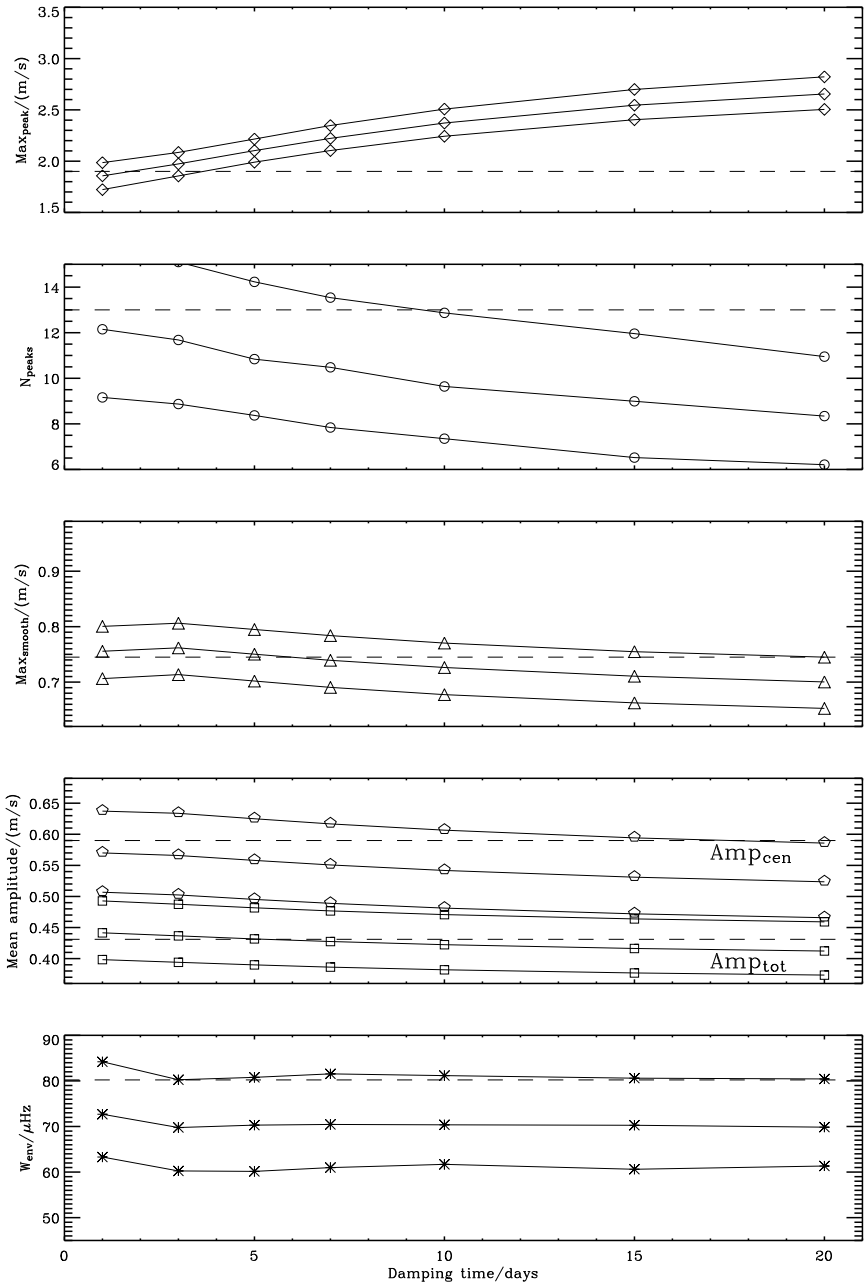

Figure 9. The effect of changing the envelope width. These panels are similar to those plotted in Fig. 6, but for three different values of envelope width. Each measured parameter is therefore shown as three points for every damping time. The input widths (from bottom to top in each panel) are: $x = 2$ (FWHM$_{\rm in} = 48.0\,\mu$Hz) (as in Fig. 6), $x = 1.2$ (FWHM$_{\rm in} = 64.0\,\mu$Hz), and $x = 0.7$ (FWHM$_{\rm in} = 81.6\,\mu$Hz). All parameters show an increase as the envelope width increases.

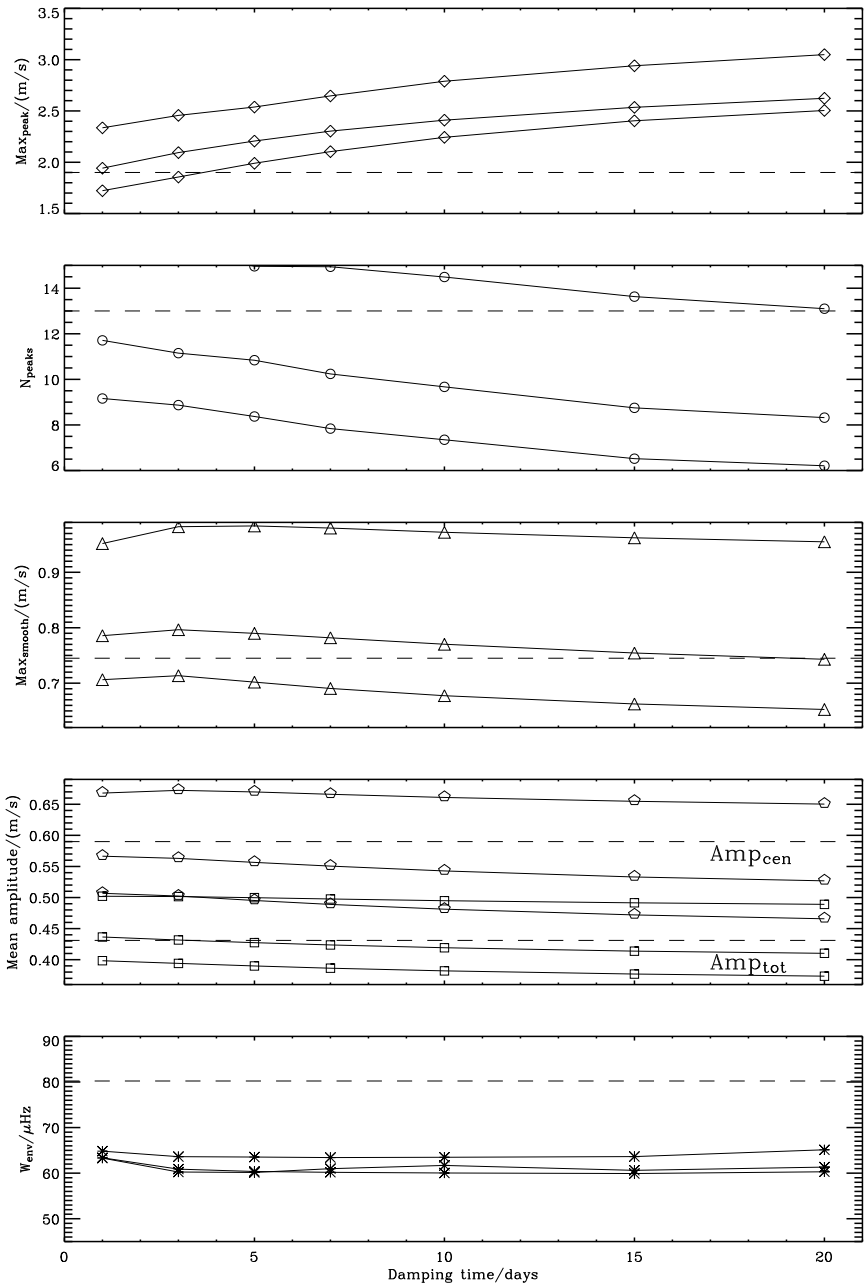

Figure 10. The effect of changing the number of input frequencies. These panels are similar to those plotted in Fig. 6, but for three different values of the frequency separation. Each measured parameter is therefore shown as three points for every damping time. The frequency separations (from bottom to top in each panel) are: 6.8 μHz (as in Fig. 6), 5.0 μHz, and 3.4 μHz. All parameters show an increase as the frequency separation decreases. The 3.4 μHz simulations corresponds to having one non-radial mode per radial mode positioned halfway between each radial mode.

4.4. Envelope width

Another way of injecting more power into the simulations, enabling more peaks to be detected without having $\mathrm{Max_{peak}}$ increase significantly, is by making the envelope wider (cf. Fig. 2). Figure 9 shows the dependence of the measured parameters on the envelope width. As expected, an increase in envelope width gives rise to an increase in all parameters, due to the power increase. $\mathrm{Max_{peak}}$ is, however, nearly unaffected. Thus, by increasing the width we construct simulations from which more peaks are detected ($\mathrm{N_{peaks}}$ increases), without affecting $\mathrm{Max_{peak}}$, hence making the simulations better fit the observations, which is also supported by the bottom panel. Since the input width is the only input parameter to induce significant changes in $\mathrm{W_{env}}$, we see from the bottom panel that the input width can be fixed at a value around $80\,\mu$Hz.

4.5. Input frequencies

Finally, we tested the dependence of the measured parameters on the number of input frequencies. The above examples have included only the radial modes, so we have simulated the presence of non-radial modes by decreasing the mean frequency separation. Since we used the radial modes from a pulsation model (Stello, 2002), they showed a small scatter of $0.2\,\mu$Hz from perfectly uniform spacing. This scatter was kept constant as we reduced the frequency separation and included more frequencies.

The results of the change in frequency separation are shown in Fig. 10. As expected we see an increase in all measured parameters when increasing the number of input frequencies (decreasing the frequency separation), due to the increase in the power, although $\mathrm{W_{env}}$ is nearly unaffected.

4.6. Finding the optimum input parameters

We find the most likely damping time by examining $\mathrm{Max_{peak}}/\mathrm{Max_{smooth}}$, which is relatively insensitive to $\mathrm{Amp_{scale}}$, envelope width, input frequencies, and noise, but not to the damping time (see Fig. 11). Thus the properties of the amplitude spectra we measure with the ratio $\mathrm{Max_{peak}}/\mathrm{Max_{smooth}}$ are mainly determined by the damping time. This ratio therefore provides a robust measure of the damping time, although it is not very precise (due to scatter). From Fig. 11 we see that the most likely damping time, given the observations, is $d \simeq 2\,$days. In Fig. 12 we show the results of simulations with a set of input parameters optimized for $d \sim 2$–$3\,$days while having the envelope fixed at

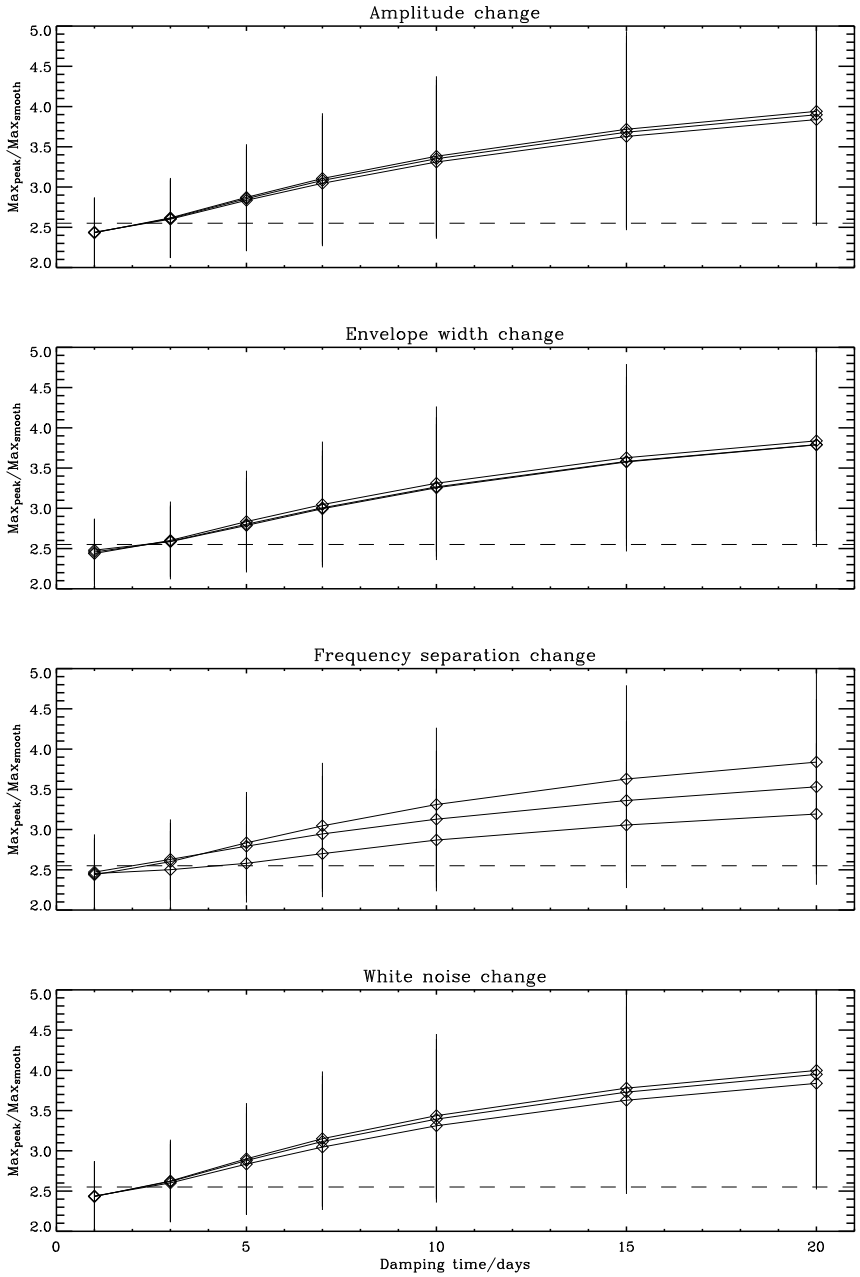

Figure 11. The ratio $\mathrm{Max_{peak}}/\mathrm{Max_{smooth}}$ as a function of damping time. The four panels show the sensitivity of $\mathrm{Max_{peak}}/\mathrm{Max_{smooth}}$ to changes to the different input parameters. The values of the input parameters are the same as shown in the former figures in Sect. 4.

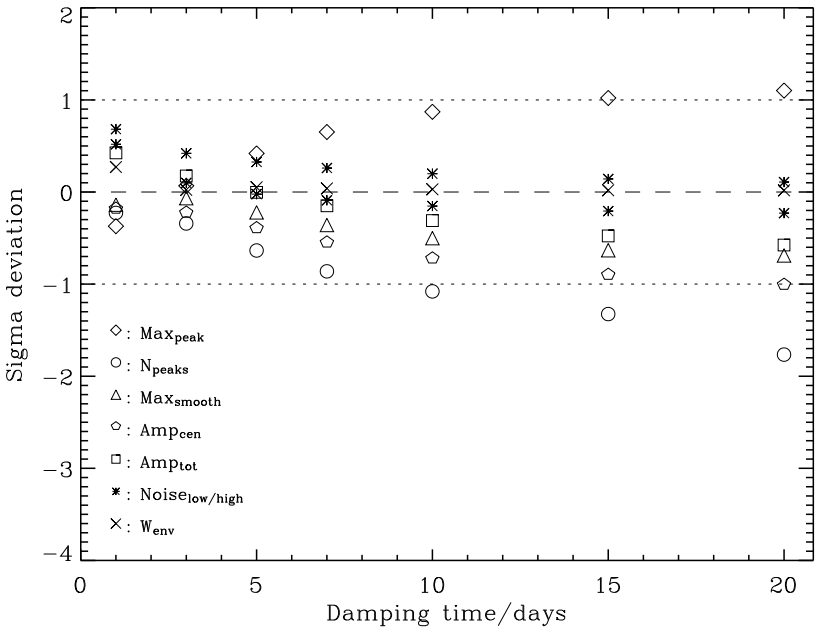

Figure 12. The deviation between observations and simulations relative to the rms scatter of the simulations (sigma deviation) of all eight measured parameters as a function of input damping time. The input parameters (optimized for $d \sim 2$–3 days) are: $\mathrm{Amp_{scale}} = 2.0\,\mathrm{m/s}$, $x = 0.7$ ($\mathrm{FWHM_{in}} = 81.6\,\mu\mathrm{Hz}$), $\mathrm{Noise_{white}} = 0.10\,\mathrm{m/s}$, $\mathrm{Noise_{slope}} = 1.5$, $\mathrm{Noise_{scale}} = 3.0$, and 18 input frequencies with a mean frequency separation of $6.8\,\mu\mathrm{Hz}$.

$\mathrm{FWHM_{in}} = 81.6\ \mu\mathrm{Hz}$ (cf. Sect. 4.4). All eight parameters are plotted in a single plot by showing the difference between observations and simulations relative to the rms scatter in the simulations. We find the most likely amplitude of ξ Hya to be $\mathrm{Amp_{scale}} \sim 2.0\,\mathrm{m/s}$.

When we optimized the input parameters for a damping time of ~ 15 days, we got roughly the same result as shown in Fig. 12. Changing the amplitude or the number of frequencies does not change $\mathrm{Max_{peak}}$ and $\mathrm{N_{peaks}}$ without also affecting the other parameters and worsening the fit (cf. Figs. 8 and 10). The problem with a damping time of $\sim$ 15 days or longer is that we cannot produce enough high peaks while keeping the other measures of power down at the observed level.

It is possible to include a few extra modes (in addition to the 18 modes with mean frequency separation $6.8\,\mu\mathrm{Hz}$) in the simulations and still have an acceptable fit with the observations because the change in the measured parameters is small, relative to the scatter, provided we also reduce the input amplitude slightly (see Figs. 8 and 10).

5. Discussion and conclusion

We have, in the previous sections, described a method for generating realistic simulations of stochastically excited oscillations, including an arbitrary noise function and an arbitrary window function. Using time series produced by our simulator we showed how the damping time, amplitude, and other mode properties of the oscillations could be determined by comparing the overall structure of observed and simulated amplitude spectra. The method was applied to the single-site time series of radial velocity measurement of the red giant star ξ Hya (Stello, 2002; Frandsen et al., 2002).

Due to the stochastic nature of the simulated solar-like oscillations, we see large variations in the amplitude spectra when the length of the time series is not significantly ($\gtrsim 10$ times) longer than the damping time. Hence, a large scatter is induced for some of the measured parameters that describe the characteristics of the amplitude spectra (see Fig. 6). In the case of ξ Hya, we are therefore not able to exclude the damping time of $\sim$ 15–20 days calculated by Houdek and Gough (2002). However, based on this single dataset, a shorter damping time of only a few days seems much more likely (see Fig. 12 *diamonds* and *circles*). A clear rejection of a damping time of 15 days or longer would require a reduction of the scatter seen in, e.g., Fig. 11 by at least a factor of two, and hence, using single-site observations, a time series of ~ 150 days (assuming that the measured parameters from the observations are unchanged). The optimum fit to the observations, assuming purely radial modes, gave a maximum amplitude ~ 2.0 m/s, in good agreement with the calculations by Houdek and Gough (2002), and damping time $\sim$ 2–3 days. Also, due to scatter, it was not possible to exclude the presence of a few extra modes beside the 18 modes with mean frequency separation 6.8 μHz. Since the theoretical calculations of the mode inertia (Teixeira, 2002) show that the radial modes should be excited to larger amplitudes than the higher degree modes, we conclude that our simulations strongly suggest that the ξ Hya amplitude spectrum is dominated by radial modes, but with a possible presence of a few higher order modes.

Below we itemize the limitations of the current investigation and discuss their consequences:

- Our approximation of using a damping time that does not vary with frequency underestimates the damping time for low frequency modes (by creating more peaks) while overestimating the damping time at the high frequency end (producing fewer peaks) relative to the theoretical damping rate (Houdek and Gough (2002); Fig.1).

Hence, due to these opposing effects, this should have little effect on our results.

- We included non-radial modes by assuming that they were excited to the same amplitudes as the radial modes in the same frequency range. A comprehensive treatment of the non-radial modes should include both the relative mode inertia, based on a pulsation model, and the spatial response of the observations due to projection effects for modes of different degree. The technique presented in this paper to measure mode life time is probably not sensitive enough to make worthwhile a more comprehensive treatment of the non-radial modes.

- We tested for any significant effect from the adopted deviation of the frequencies from equal spacing by testing both the scatter of $0.2\,\mu$Hz seen in the pulsation model (as in the examples shown in Sect. 4) and the larger scatter ($0.6\,\mu$Hz) seen when the observed frequencies were ordered to match the radial modes (see Stello, 2002). In these two cases, the eight measured parameters were found to be nearly unchanged, with a deviation of less than 0.1σ, which is the precision with which we know the mean values based on 100 independent simulations.

  Furthermore, we tested a very irregular frequency distribution by using the 13 observed peaks with S/N$\geq$ 3.5 (see Stello, 2002) as input frequencies, neglecting possible contamination from alias peaks and noise. The results are similar to those shown in Sect. 4.

  We conclude that the regularity in the input frequencies is not important for obtaining our current result.

- The observed velocities of ξ Hya were reduced using one reference point per night, which produced a high-pass filtering of the time series (Frandsen et al., 2002). It would presumably require somewhat different values of the input parameters to match the unfiltered amplitude spectrum. We expect this would mostly affect the input noise and amplitude, by underestimating them, and to a lesser extent the damping time.

- We chose to use the smoothed observed amplitude spectrum as the frequency envelope because it represents the actual observations. We expect that a Gaussian profile could be used for simplicity with little effect on the results.

- We used two successive relatively narrow boxcars to smooth the amplitude spectrum in order to obtain $\mathrm{Max}_{\mathrm{smooth}}$. This method

preserved the large-scale structure while removing variations on small scales. Increasing the boxcar widths by a factor of 2 or 3 did not produce any significant change in the difference between $\mathrm{Max}_{\mathrm{smooth}}$ of simulations and observations.

- To test the robustness of our method we applied it to measurements in velocity of α Cen A (Butler et al., 2004). Based on a plot similar to Fig. 11, we obtain a damping time of $\sim$ 0–5 days. A complete analysis, as shown for ξ Hya, has not been applied to α Cen A. Since α Cen A is very similar to the Sun, one would expect the damping time to be only a few days. Our result is consistent with both the solar value (3–4 days) and the value of 1–2 days for α Cen A found by Bedding et al. (2004).

In general, we see from our simulations that when comparing the estimated amplitude (either from scaling or theoretical calculations) with observations, the amplitude associated with a star from a single dataset can vary significantly, especially for stars with mode life times that are long compared to the length of the time series (cf. Fig. 6).

In a future paper, a more detailed frequency analysis of ξ Hya will be presented, including an analysis of the scatter of frequencies about a uniform distribution, which would test the damping time results given in this paper.

Acknowledgements

This work was supported in part by the Australian Research Council, the Danish National Research Foundation through its establishment of the Theoretical Astrophysics Center, and by the Fund for Scientific Research of Flanders through a post-doctoral fellowship of Joris De Ridder and through grant G.0178.02.

References

Bedding, T. R. and H. Kjeldsen: 2003, 'Solar-like Oscillations'. *Publications of the Astronomical Society of Australia* **20**, 203–212.

Bedding, T. R., H. Kjeldsen, R. P. Butler, C. McCarthy, G. W. Marcy, S. J. O'Toole, C. G. Tinney, and J. T. Wright: 2004, 'Oscillation frequencies and mode lifetimes in α Centauri A'. ApJ, submitted.

Brown, T. M., R. L. Gilliland, R. W. Noyes, and L. W. Ramsey: 1991, 'Detection of possible p-mode oscillations on Procyon'. *ApJ* **368**, 599–609.

Butler, R. P., T. R. Bedding, H. Kjeldsen, C. McCarthy, S. J. O'Toole, C. G. Tinney, G. W. Marcy, and J. T. Wright: 2004, 'Ultra-high-precision velocity measurements of oscillations in alpha Cen A'. ApJ lett., in press, astro-ph/0311408.

Chang, H.-Y. and D. O. Gough: 1998, 'On the Power Distribution of Solar P MODES'. *Sol. Phys.* **181**, 251–263.

De Ridder, J.: 2002, 'Time Series Simulator'. Technical report, Rømer Science Data Center, Aarhus Universitet.

De Ridder, J., H. Kjeldsen, T. Arentoft, and A. Claret: 2003, 'The EDDINGTON Light Curve Simulator'. In: *Stellar Structure and Habitable Planet Finding.* in press.

Frandsen, S., F. Carrier, C. Aerts, D. Stello, T. Maas, M. Burnet, H. Bruntt, T. C. Teixeira, J. R. de Medeiros, F. Bouchy, H. Kjeldsen, F. Pijpers, and J. Christensen-Dalsgaard: 2002, 'Detection of Solar-like oscillations in the G7 giant star ξ Hya'. *A&A* **394**, L5–L8.

Goldreich, P. and D. A. Keeley: 1977, 'Solar seismology. II - The stochastic excitation of the solar p-modes by turbulent convection'. *ApJ* **212**, 243–251.

Houdek, G., N. J. Balmforth, J. Christensen-Dalsgaard, and D. O. Gough: 1999, 'Amplitudes of stochastically excited oscillations in main-sequence stars'. *A&A* **351**, 582–596.

Houdek, G. and D. O. Gough: 2002, 'Modelling pulsation amplitudes of ξ Hydrae'. *MNRAS* **336**, L65–L69.

Kjeldsen, H.: 2003, 'Space and Ground Based Data for Asteroseismology'. *Ap&SS* **284**, 1–12.

Kjeldsen, H. and T. R. Bedding: 1998, 'MONS: A proposal for a Danish satellite'. In: *The First MONS Workshop: Science with a Small Space Telescope, held in Aarhus, Denmark, June 29 - 30, 1998, Eds.: H. Kjeldsen, T.R. Bedding, Aarhus Universitet, p. 1.* pp. 1–+.

Kjeldsen, H. and S. Frandsen: 1992, 'High-precision time-resolved CCD photometry'. *PASP* **104**, 413–434.

Leifsen, T., B. N. Andersen, and T. Toutain: 2001, 'Temporal behaviour of radial p-modes'. In: *ESA SP-464: SOHO 10/GONG 2000 Workshop: Helio- and Asteroseismology at the Dawn of the Millennium.* pp. 63–+.

Priestley, M. B.: 1981, *Spectral analysis and time series*, Vol. 1 of *Probability and mathematical statistics.* London; New York: Academic Press.

Stello, D.: 2002, 'Detecting solar-like oscillations in the giant star ξ Hydrae. New prospects for asteroseismology throughout the HR-diagram'. Master's thesis, Institut for Fysik og Astronomi, Aarhus Universitet. Available HTTP: http://www.phys.au.dk/∼stello/Publications/thesis.pdf.

Teixeira, T. C.: 2002. Private communication; work in progress.